

Seeing Is Knowing! Fact-based Visual Question Answering Using Knowledge Graph Embeddings

Kiran Ramnath and Mark Hasegawa-Johnson

Department of Electrical and Computer Engineering,
University of Illinois, Urbana-Champaign
kiranr2@illinois.edu, jhasegaw@illinois.edu

Abstract

Fact-based Visual Question Answering (FVQA), a challenging variant of VQA, requires a QA-system to include facts from a diverse knowledge graph (KG) in its reasoning process to produce an answer. Large KGs, especially common-sense KGs, are known to be incomplete, i.e. not all non-existent facts are always incorrect. Therefore, being able to reason over incomplete KGs for QA is a critical requirement in real-world applications that has not been addressed extensively in the literature. We develop a novel QA architecture that allows us to reason over incomplete KGs, something current FVQA state-of-the-art (SOTA) approaches lack. We use KG Embeddings, a technique widely used for KG completion, for the downstream task of FVQA. We also employ a new image representation technique we call ‘Image-as-Knowledge’ to enable this capability, alongside a simple one-step co-Attention mechanism to attend to text and image during QA. Our FVQA architecture is faster during inference time, being $O(m)$, as opposed to existing FVQA SOTA methods which are $O(N \log N)$, where $m = \text{number of vertices}$, $N = \text{number of edges} = O(m^2)$. We observe that our architecture performs comparably in the standard answer-retrieval baseline with existing methods; while for missing-edge reasoning, our KG representation outperforms the SOTA representation by 25%, and image representation outperforms the SOTA representation by 2.6%.

Introduction

Multi-modal reasoning has been a prime focus in the pursuit of artificial general intelligence. One such task is Visual Question Answering (Antol et al. 2015; Goyal et al. 2017), which requires the system to answer a textual question based on an image. VQA is challenging because it requires many capabilities such as object detection, scene recognition, activity recognition, language understanding, and common-sense reasoning. (Wang et al. 2018) noted that most of the questions in the VQA dataset didn’t require common-sense knowledge residing outside of the image. For instance, they found that only 5.5% of questions required adult-level knowledge to answer. Humans have a remarkable ability to blend in knowledge from their own prior experiences when answering a question about an image. With this motivation, Wang et. al therefore introduced the FVQA benchmark, aiming to provide a more challenging set of questions which



Figure 1: Example of a fact-based visual question
Question - Which object in this image is rich in potassium?
Supporting fact - Bananas are rich in potassium
SPO triple - (Bananas, HasProperty, rich in Potassium)
Answer Source - Image
Answer - Bananas

ensure that the answer to a given question requires some form of external knowledge, not present in the image or the question text. They provide this external information in the form of knowledge graphs, which are multi-relational graphs, storing relational representations between entities. The task of FVQA boils down to retrieving the correct entity as the answer most relevant to an image. For example, in Fig. 1 the fact triple – (Banana, HasProperty, rich in Potassium) is the external information required to answer the question; with the correct answer being ‘Banana’.

The primary contribution of this paper is a method that permits FVQA to reason about common-sense facts that are absent from the knowledge graph (missing edges). KG embeddings permits us to offer two additional contributions to the SOTA in FVQA: an ‘image-as-knowledge’ representation of visual information, and a coAttention method for combining visual and textual inputs. ‘Image-as-knowledge’ represents the image as the span of the KG embedding vectors for the entities found in it. It is more effective than a ‘bag-of-words’ image representation, because the ‘image-as-knowledge’ vectors encode information about the graph structure. CoAttention uses the words of the query to compute weighted combinations of the entity vectors, in effect a vector within the span of the image entities. Two such iden-

tical models are trained separately, which are gated in order to query the entities in the KG during inference. The practical result of these methods is an accurate FVQA system that does not lose its accuracy when the required edge is missing from the KG. Finally, our architecture is more time-efficient during inference, being $O(m)$ as it only needs to reason over existent nodes in the network. Existing SOTA methods (Narasimhan, Lazebnik, and Schwing 2018), on the other hand, involve ranking facts (i.e. edges in the network) and are therefore $O(n \log n)$, where $n = \text{number of edges} = O(|R| m^2)$, where $|R|$ is the number of different types of edges that can exist in the dataset. To the best of our knowledge, our work is the first one to apply KG embeddings to a VQA task.

Related Work

Knowledge Graphs Knowledge graphs (Suchanek, Kasneci, and Weikum 2007; Auer et al. 2007; Mitchell and Fredkin 2014; Bollacker et al. 2008; Dong et al. 2014) have been studied as an effective way of representing objects or concepts and their inter-relationships. Such relational representations are formally defined in the RDF (Resource Description Framework) as triples $f = (\text{subject}, \text{predicate}, \text{object})$, where $(\text{subject}, \text{object})$ are entities, predicate is the relation connecting the two entities. Such linked representations have been found to correlate highly with how humans process cognitive information (Halford, Wilson, and Phillips 2010).

KG embeddings: Common-sense KGs extracted from web-scale datasets are usually incomplete. KG embedding techniques (Bordes et al. 2013; Sun et al. 2019; Socher et al. 2013; Nickel, Tresp, and Kriegel 2011; Dong et al. 2014; Dettmers et al. 2018) have been studied as a means to remediate incompleteness of large-scale KGs. Score-based latent feature models, which perform well on several benchmarks, learn a score mapping $\phi(h, r, t) : \mathcal{E} \times \mathcal{R} \times \mathcal{E} \rightarrow \mathbf{R}$ where \mathcal{E} is the set of all entities, \mathcal{R} is the set of all relation-types. $h, t \in \mathcal{E}$ are the head (subject) and tail (object), $r \in \mathcal{R}$ is the relation. $\mathcal{G} \subset \mathcal{E} \times \mathcal{R} \times \mathcal{E}$ is the observed set of edges, while $\mathcal{G}_o \supset \mathcal{G}$ is the unknown set of true edges. The embeddings (h, r, t) are learned so that the score $\phi(\cdot)$ is high for edges in \mathcal{G}_o , and low for edges in its complement.

Distance-based models (Bordes et al. 2013; Sun et al. 2019; Trouillon et al. 2016; Bordes et al. 2011) learn embeddings h , r and t in order to minimize the distance between t and $f(h, r)$, for some projection function $f(\cdot)$. Our study for FVQA explores the use of two such distance-based models: TransE (Bordes et al. 2013) and RotatE (Sun et al. 2019). TransE models $f(h, r) = h + r$. RotatE models $f(h, r)$ as a Hadamard product, $h \circ r$, where the embedding vectors h , r and t are in the complex plane and r is enforced to be unit norm, so that $h \circ r$ is a rotation in the complex plane. While distance-based models are scalable, they are only effective if each entity has adequate training data. Common-sense KGs are often based on free text, therefore most entities occur rarely; an example is the entity “rich in potassium” in Fig. 1. For this reason, few baselines have been studied for this task (Li et al. 2016; Malaviya et al. 2020). A suitable model

we study for our KG completion task is the Entity-Relation Multi-Layer Perceptron (ERMLP) (Dong et al. 2014). It uses an MLP to produce the score $\phi(h, r, t)$ for each fact triple.

FVQA: The fact-based visual question answering (FVQA (Wang et al. 2018)) benchmark was designed using questions that obey the following condition: for each (question,image,answer) triplet in the dataset $((q_i, I_i, y_i) \in \mathcal{D})$, there exists exactly one supporting fact in the knowledge graph $(f_j = (h, r, t) \in \mathcal{G})$ such that the correct answer y_i is either the head or the tail of f_j , and such that at least one of the two entities is visible in the image.

The accompanying KG is also diverse, comprising facts from three individual KGs: Webchild (Tandon et al. 2014), ConceptNet (Liu and Singh 2004), and DBpedia (Auer et al. 2007). DBpedia provides parent-child relationships between different entities, ConceptNet provides common-sense knowledge about entities, whereas Webchild provides many different kinds of comparative relationships between entities (comparative relations are considered as a single relationship type for FVQA). In total, the dataset contains 13 relations: $R \in \{\text{Category}, \text{HasProperty}, \text{RelatedTo}, \text{AtLocation}, \text{IsA}, \text{HasA}, \text{CapableOf}, \text{UsedFor}, \text{Desires}, \text{PartOf}, \text{ReceivesAction}, \text{CreatedBy}, \text{Comparative}\}$. The dataset consists of 2190 images sampled from the ILSVRC (Russakovsky et al. 2015) and the MSCOCO (Lin et al. 2014) datasets. The accompanying KG consists of roughly 194500 facts, concerning 88606 entities. Roughly 82% of the questions have a Key Visual Concept (KVC) as the answer, whereas the rest have some information from the Knowledge Base (KB) about a KVC as the answer.

Answering questions in FVQA is to solve for

$$\hat{y} = \underset{e \in \mathcal{E}}{\operatorname{argmax}} p(y = e \mid q, I, \mathcal{G}), \quad (1)$$

i.e., finding the most probable entity as the answer given a question q and image I , and given the graph \mathcal{G} . Our formulation of the missing edge reasoning task considers \mathcal{G}_o .

(Wang et al. 2018) attempted FVQA as a parsing and querying problem, constructing 32 different templates of queries, and classifying each image-question pair as requiring one of these templates. Simple keyword matching techniques further prunes the retrieved facts. Straight to the Facts (STTF) (Narasimhan and Schwing 2018) approached FVQA by directly learning to retrieve supporting facts, where each fact-entity was represented using lexical semantic representations. (Narasimhan, Lazebnik, and Schwing 2018) extended this approach in Out-of-the box (OOB), the current SOTA, by using local neighbourhood-based reasoning via a Graph Convolution Network (GCN) (Kipf and Welling 2017) to answer each question. OOB answers the query by constructing a subgraph based on the query and image, then applying GCN reasoning to the subgraph; the subgraph construction stage has an inference time complexity of $O(n \log n)$. The GCN models local interactions through message passing between nodes, but potentially ignores global structures that could be useful for this task. All of these current approaches rely on the ground-truth fact to be present in the KG. A real-world application, however, is likely to generate questions that are not supported by any single fact

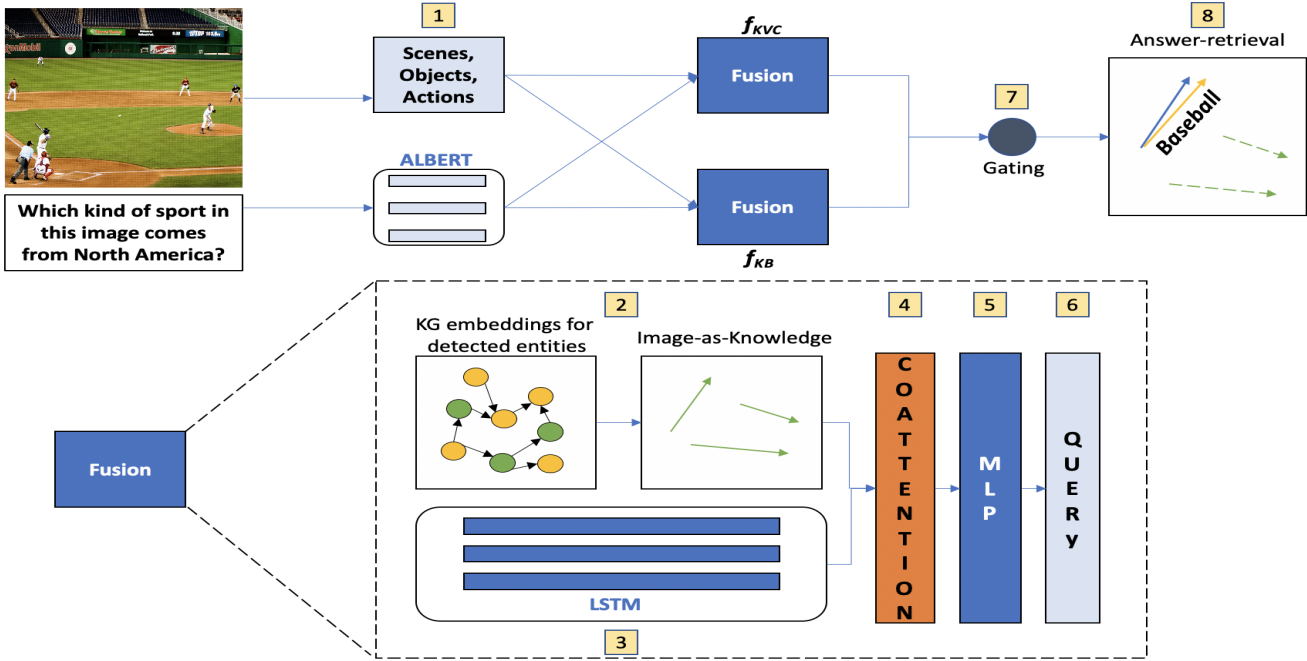


Figure 2: Our inference architecture for FVQA. (1) Scenes, objects, & actions are detected in the image. (2) For detected entities, we retrieve their KG embedding representations. The span of these embedding vectors represents the ‘image-as-knowledge’. (3) Lexical semantic vectors for each word in the query are accumulated via an LSTM. (4) The joint image-question encoding is derived using a coAttention mechanism described in Fig. 3, then (5) passed through a multi-layer perceptron, whose (6) last layer is used as a pair of queries that are (7) gated, and (8) used to retrieve the entity to answer the question.

present in the KG. Our architecture is an attempt to address this shortcoming.

Our approach

The proposed architecture for FVQA is shown in Fig. 2. As shown, a given image I and query q are combined via coAttention to form two entity query vectors, $f_{KVC}(q, I)$ and $f_{KB}(q, I)$. The KG is then queried for the answer, according to

$$\hat{y}(q|I) = \begin{cases} \operatorname{argmax}_{e \in \mathcal{E}} f_{KVC}(q, I)^T e & g_{KVC}(q) = 1 \\ \operatorname{argmax}_{e \in \mathcal{E}} f_{KB}(q, I)^T e & g_{KVC}(q) = 0 \end{cases} \quad (2)$$

where the gating function $g_{KVC}(q) \in \{0, 1\}$ is equal to 1 if the text of the question indicates that the answer is visible in the image, equal to 0 otherwise. The rest of this section addresses representations of the entities, image, and query, the information fusion functions, the gating function, and the loss function.

KG representation: We perform negative mining to set up the surrogate binary classification task to learn KG embeddings. Not all edges absent from \mathcal{G} are false, but under the empirically observed Local Closed World Assumption (Galárraga et al. 2013; Dong et al. 2014), it has been found that samples generated by randomly corrupting tail entities for a given (h, r) pair are very rarely true. (Cai and Wang 2018) found that such negative samples may

often be too easy to classify as false. (Sun et al. 2019) proposed a self-adversarial negative sampling strategy, in which the adversarial examples $f'_j = (h_i, r_i, t'_i)$ generated from each observed edge $f_i = (h_i, r_i, t_i)$ are weighted by their truth probability as estimated by the learned embeddings h and t , and by the corresponding score function $\phi(h, r, t)$. A total of n adversarial examples are generated for each positive example, and used to train discriminative embeddings using noise contrastive estimation (Gutmann and Hyvärinen 2010). Thus the knowledge graph embedding loss \mathcal{L}_{KGE} includes the negative log probability that each observed edge is true ($\ln \sigma(\phi(f_i))$), and the expected log probability that the adversarial edges are false ($\ln \sigma(-\phi(f'_j)) = \ln(1 - \sigma(\phi(f'_j)))$):

$$\mathcal{L}_{KGE} = - \sum_{i=1}^{|\mathcal{G}|} (\ln \sigma(\phi(f_i)) + E_i [\ln \sigma(-\phi(f'_j))]), \quad (3)$$

where expectation is with respect to the probability $p_i(f'_j)$, tuned using a temperature hyperparameter α as

$$p_i(f'_j) = \frac{\exp(\alpha \phi(f'_j))}{\sum_{k=1}^n \exp(\alpha \phi(f'_k))} \quad (4)$$

Eq. (3) is used to train embeddings of the head (h) and tail (t), which are applied to the FVQA task as described in the next several subsections. Eq. (3) also trains relation embed-

dings (r) and MLP weights for the ERMLP scoring function (w_{MLP}); these quantities are not used for the downstream FVQA task.

Image representation: Narasimhan et. al found that providing raw feature maps from a standard convolutional network like ResNet (He et al. 2016) or VGG (Simonyan and Zisserman 2015) actually hurt performance on FVQA. We therefore represent each image using visual concepts found in the image.

Objects - We use Torchvision’s Coco object-detector, a Faster RCNN detector (Ren et al. 2015) with ResNet50 backbone (He et al. 2016), and feature pyramid network (Lin et al. 2017), which detects 80 object classes. We also use a detector (ZFTurbo 2018) trained on OpenImages 600 classes detections; considering those classes which are present in ImageNet 200 object detection classes as well as (Wu et al. 2016) to find maximal overlap with the dataset used with FVQA.

Scenes – We use a wideresnet (Zagoruyko and Komodakis 2016) detector trained on MIT365 places dataset (Zhou et al. 2017) and consider the 205 classes that were used in constructing the FVQA KG. Overall, we detect 540 image-classes or Visual Concepts.

To ensure we have access to similar detections as the baselines and allow us to fairly study the effects of our main contributions downstream, we ensure that the Ground-Truth answer entities are present as visual concepts in each image. This does not make the downstream task of answer detection any easier, since we are still performing a search over the space of all entities, i.e. over roughly 88,000 entities. We find that not using these detections leads to a drop in accuracy for all methods on our architectures. For a fair evaluation, we use the same detections for all our ablation studies and our implementation of the baseline.

Having detected visual concepts in each image, we represent each image as a bag of entities. More specifically, $I_i = [e_i^1, \dots, e_i^m] \in \mathbf{R}^{N_e \times m}$, where N_e is the embedding dimension, and m is the number of visual concepts detected in the image. We detect a maximum of $m = 14$ visual concepts in each image. Our findings imply that for FVQA reasoning, an image is best represented as a collection of KG concepts, apparently because these concept representations encode the graph structure and background information necessary to be able to answer questions. We think this is an important finding, and we show its effect on the answer prediction accuracy.

Language representation: For representing words in the question, we make use of contextual word embeddings. We use ALBERT embeddings (Lan et al. 2020), specifically the last layer’s encodings for each word, taken in the context of the entire question. We do not train the contextual word embeddings but use them as inputs for an LSTM (Hochreiter and Schmidhuber 1997). After passing through the LSTM, we use the hidden state representation for each word w for further processing as $q_i^t = h(w_t)$ as the question representation.

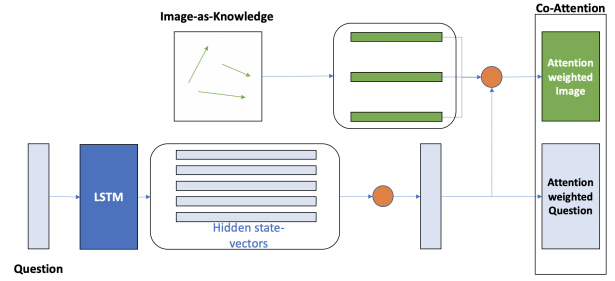


Figure 3: Image and query are fused using the CoAttention mechanism depicted here. First, self-attention computes a weighted summary of the query (bottom orange circle). Second, the query is used to compute an attention-weighted summary of the concepts in the image (top orange circle). The resulting image query is a vector drawn from the span of the entities present in the image.

Fusion Functions f_{KVC} and f_{KB} : Image and query are fused using a CoAttention mechanism, as depicted in Fig. 3. First, we calculate attention weights for each word in the question, and subsequently an attention-weighted encoding for the question as:

$$A(q_i) = \sum_{t=1}^{|q_i|} \alpha_q^t q_i^t, \quad \alpha_q^t = \frac{\exp(w_{\alpha_q}^T q_i^t)}{\sum_{t=1}^{|q_i|} \exp(w_{\alpha_q}^T q_i^t)} \quad (5)$$

where α_q^t, w_{α_q} are respectively the attention paid to word w_t , and the weight vector from which it is computed. $A(q_i)$ is the attention-weighted representation of the question. We do not use any query vector for the question, and therefore the attention-weights could be interpreted as relevance-scores for words in a given question.

Then, using $A(q_i)$ as a query, we compute an attention-weighted summary of the image:

$$A(I_i) = \sum_{j=1}^m \alpha_I^j e_i^j, \quad \alpha_I^j = \frac{\exp\left(w_{\alpha_I}^T \begin{bmatrix} A(q_i) \\ e_i^j \end{bmatrix}\right)}{\sum_{k=1}^m \exp\left(w_{\alpha_I}^T \begin{bmatrix} A(q_i) \\ e_i^k \end{bmatrix}\right)} \quad (6)$$

where $\alpha_I^j, w_{\alpha_I}, e_i^j$ are respectively the attention paid to concept j in the image, the weight vector from which it is computed, and the j^{th} concept present in the image. $A(I_i)$ is the attention-weighted representation of the image. Both $A(I_i)$ and $A(q_i)$ learn a mapping: $R^{N_e \times m} \rightarrow R^{N_e}$, which is the attention-based weighted average of its inputs, thus $A(I_i)$ is a vector drawn from the span of the entities present in the image.

These attention-weighted image and question encodings compute joint image-question encodings via late fusion, as:

$$f_{KVC}(q_i, I_i) = h(A(I_i), A(q_i); w_{KVC}) \quad (7)$$

$$f_{KB}(q_i, I_i) = h(A(I_i), A(q_i); w_{KB}) \quad (8)$$

where $h(\cdot)$ is a two-layer fully-connected network with ReLU activation functions. One of the ablations we tested experimentally uses $f_{KVC}(q_i, I_i) = A(I_i)$, i.e., the attention weighted image encodings directly retrieve the answer

Parameters	Description	Loss Function
h, r, t, w_{MLP}	For ERMLP embeddings	\mathcal{L}_{KGE} and \mathcal{L}_{FVQA}
h, r, t	For TransE embeddings	\mathcal{L}_{KGE} and \mathcal{L}_{FVQA}
h, r, t	For RotatE embeddings	\mathcal{L}_{KGE} and \mathcal{L}_{FVQA}
$w_{\alpha_q}, w_{\alpha_I}, w_{KVC}, w_{KB}, \theta_{LSTM}$	For answer-retrieval based on image and question	\mathcal{L}_{FVQA}
w_g, θ_{LSTM}	Choose answer source $\in \{f_{KVC}, f_{KB}\}$	Binary cross entropy

Table 1: Summary of all trainable parameters. Head (h) and tail (t) use identical embedding vectors for identical entities. Relation embeddings (r) and ERMLP weights (w_{MLP}) are co-trained with h and t , but not used for the downstream FVQA.

Method	Sampling	MR	MRR	Hits@1	Hits@3	Hits@10
TransE	adversarial	14692	0.1035	0.05	0.13	0.19
TransE	uniform	13736	0.0967	0.04	0.112	0.194
RotatE	adversarial	17660	0.173	0.14	0.18	0.22
RotatE	uniform	18468	0.144	0.122	0.152	0.179
ERMLP	adversarial	11194	0.156	0.132	0.152	0.197
ERMLP	uniform	14907	0.122	0.09	0.128	0.173
ERMLP (missing edges)	adversarial	11071 ± 479	0.162 ± 0.007	0.136 ± 0.003	0.162 ± 0.005	0.204 ± 0.007

Table 2: KG Embedding accuracy

to the question. This ablation significantly reduces accuracy, suggesting the need for successive fully connected layers to add capacity to the network’s reasoning process.

Gating function g_{KVC} : The fusion functions f_{KVC} and f_{KB} are trained to retrieve two different entities from the KG, either of which might be the answer to the question. The gating function, g_{KVC} , selects one of these two. The gating function is a sigmoid fully-connected layer applied to the final output state of an LSTM, whose input is the query, and which is trained using binary cross entropy so that $g_{KVC} = 1$ if the correct answer is a key visual concept in the image.

Loss function: A summary of all parameters is provided in Table 1. Entity embeddings are learned in order to minimize the loss function in Eq. (3), then all parameters are jointly trained in order to minimize the cosine distance between the ground truth entity, y_i , and the network output:

$$\mathcal{L}_{FVQA} = \sum_i (1 - y_i^T \hat{y}(q_i | I_i)) \quad (9)$$

where $\hat{y}(q_i | I_i)$ is as given in Eq. (2).

Experimental Setup

KG Embeddings training: For training of each KG embedding algorithm, we split all the facts in the KG as 80% train, 20% test. Additionally, for the experiments on missing-edge reasoning, we ensure that the supporting facts for questions in the validation set are removed from the KGE training set as well. Entity and relation embeddings have a dimension of $N_e = 300$. For RotatE, this means that the real and imaginary spaces each have 150 dimensions. Batch size is 1000. Each network is trained for 25000 steps using the Adam optimizer with learning rate shrunk every 10000 steps by 0.1. TransE and RotatE use $\gamma = 24$ and learning rate of 0.0001. ERMLP uses $\gamma = 12$ and learning rate of 0.01. We set $\alpha = 1$ for all experiments. For all models in this section and the next, we tried starting learning rates in

the set {0.1, 0.01, 0.001, 0.0001}. We use $n = 16$ negative samples for each positive sample. ERMLP uses a three layer neural network. The input layer has dimension $3N_e$ (taking in head, rel, and tail embeddings), the hidden layers have $2N_e = 600$ and $N_e = 300$ units respectively, and the output contains one unit (the score $\phi(h, r, t)$). Hidden activations are ReLU; the output uses a sigmoid as shown in Eq. (3). No dropout was used.

KGE accuracy is measured using standard metrics: Hits @1, Hits @3, Hits @10 determine how often each correct tail/head ranks in the top 1, 3, or 10 ranked facts for each ground-truth $(h, r)/(r, t)$ pair. Mean Rank measures the mean rank of each true fact in the dataset, Mean Reciprocal Rank = $\frac{1}{|\mathcal{D}|} \sum_i \frac{1}{R_i}$. While we report these metrics, we do note that these metrics are not best suited for common-sense KGs for reasons mentioned before. However we leave a more refined analysis of these methods for future work.

FVQA training: We report Hits @1 and Hits @3 for each algorithm. All numbers are based on averaging results across five train - test splits provided with the dataset. Each split includes 1100 images in training set, 1090 images in the test set. The number of questions varies slightly, but roughly fall half into both training and testing sets for each split. Stochastic gradient descent with a batch size of 64 trains f_{KVC} and f_{KB} for 250 steps with a learning rate of 0.01, reduced by 0.1 every 100 epochs, and a weight decay of 1e-3. Fully-connected layers use a dropout probability of 0.3. The gating function g_{KVC} is trained for 20 steps with step-size of 0.1.

GPUs provided by Google Colab are used to train all models. Given that the GPU assignments and server performance vary over time, we did not get a consistent running time estimate. However, our heaviest KG embedding technique (ERMLP) takes roughly 3 hours to train, while one train split for f_{KVC} takes roughly 30 minutes.

Baselines: FVQA results are compared to those of the baselines below. These results (except when noted other-

Technique	Hits@1	Hits@3
LSTM, image - SVM (Wang et al. 2018)	22.97 ± 0.64	36.76 ± 1.22
Hie-question + Image (Wang et al. 2018; Lu et al. 2016)	33.7 ± 1.18	50.00 ± 0.78
Hie-question + Image pre-VQA (Wang et al. 2018; Lu et al. 2016)	43.14 ± 0.61	59.44 ± 0.34
FVQA top-1 qq-mapping (Wang et al. 2018)	52.56 ± 1.03	59.72 ± 0.82
FVQA top-3 qq-mapping (Wang et al. 2018)	56.91 ± 0.99	64.65 ± 1.05
STTF (Narasimhan and Schwing 2018)	$62.2 \pm NR$	$75.6 \pm NR$
OOB top-1 rel (Narasimhan, Lazebnik, and Schwing 2018)	$65.8 \pm NR$	$77.32 \pm NR$
OOB top-3 rel (Narasimhan, Lazebnik, and Schwing 2018)	$69.35 \pm NR$	$80.25 \pm NR$
Our architecture		
Avg word embeddings, IaK	27.77 ± 0.72	32.43 ± 0.94
TransE, IaK	38.64 ± 1.51	52.58 ± 1.93
TransE – Adv, IaK	40.37 ± 0.87	53.1 ± 1.12
RotatE, IaK	45.59 ± 0.52	56.55 ± 1.18
RotatE – Adv, IaK	47.92 ± 1.15	61.3 ± 0.97
ERMLP -Adv, IaK	54.38 ± 0.94	65.76 ± 0.5
ERMLP, IaK	53.16 ± 0.79	$63.9 \pm .63$
ERMLP -Adv, IaK, Random entity initialization	54.1 ± 1.22	67.02 ± 1.07
ERMLP – Adv, Multihot	51.51 ± 1.14	64.89 ± 1.37
Missing edge results		
Avg Word Embeddings, IaK	27.77 ± 0.72	32.43 ± 0.94
ERMLP -Adv, IaK	53.45 ± 0.77	65.1 ± 1.41

Table 3: FVQA accuracy (IaK - Image as Knowledge, Adv - self-adversarial negative sampling, NR - Not reported)

wise) are taken from the respective papers since the codes for these systems have not been made available. **AvgEmbed:** Our implementation which tries to compare STTF’s and OOB’s fact representation methodology with our architecture to correctly perform missing-edge reasoning. We use averaged 300-dimensional GLoVE embeddings (Pennington, Socher, and Manning 2014) to represent each entity.

Results and Discussion

The gating function achieves an accuracy of 96%, same as reported in (Narasimhan and Schwing 2018). Setting $I_i = 0$ and using $f_{KB}(q_i, 0)$ to retrieve a relation, rather than an entity, achieves an average accuracy of 74%, again close to the levels reported using a softmax classifier by STTF.

Q1 - Which KG embedding algorithm performs better? ERMLP has better mean-rank, while RotatE performs better in all other standard metrics for KG embeddings. (Table 2). However, ERMLP-based embeddings are more successful for FVQA (Table 3). Apparently ERMLP adds more capacity to the embedding model, which also helps the downstream task of FVQA.

Q2 – How helpful is self-adversarial negative sampling for KG completion, and for FVQA? We see for each technique, that the accuracy improves for both the KG embedding task (Table 2) and the downstream FVQA (Table 3) upon introducing self-adversarial negative sampling during KG embedding training. The FVQA accuracy improves by 1.67%, 2.47 %, and 1.25 % respectively for TransE, RotatE, and ERMLP using self-adversarial negative sampling. (Guu, Miller, and Liang 2015) reported that initializing entity vectors as averaged word embeddings yields better per-

formance. We don’t see a significant improvement on doing so compared to randomly initializing the entity vectors.

Q3 – How helpful is representing Image-as-Knowledge with coAttention? To understand how useful the Image-as-Knoweldge representation is compared to other variants, we compare it to the multihot variant proposed by Narasimhan et. al along with our best performing KG embedding technique. ‘Image-as-knowledge’ provides a 3-point performance improvement (Table 3), apparently because the retrieval of an entity happens in the entity space spanned by the vectors of the IaK representation.

Q4 – Can the proposed architecture find an answer despite missing edges? When the required edge is present in the graph, our architecture underperforms OOB by 11%. However, for all five train-test splits, the proposed architecture is able to answer questions with the same accuracy (within $\pm 1.07\%$), regardless of whether or not the necessary fact exists in the KG. The only comparable baseline in Table 3 is our own architecture, using averaged word embeddings as queries, which underperforms by over 25%

Success and Failure cases We now turn to look at the failure modes for our architecture. Since the gating function performs with almost perfect accuracy, our main source of error is incorrect entity prediction. For the cases when f_{KVC} gives the answer, we see an accuracy of $64.42\% \pm 0.76$, whereas for f_{KB} it is only $4.45\% \pm 1.32$. Further exploration of the errors yields interesting insights. It must be reiterated that we consider an answer as correct only if there is an exact match between the entity predicted and the ground-truth. We empirically observe that this stringent but narrow requirement leads to a significant fraction of semantically



Figure 4: **Question:** What is the difference between the instrument and the violin?

SPO triple: : {Cello, HasProperty, like a violin but larger}

Answer Source: Knowledge Base

Answer: like a violin but larger

Answer predicted: like a violin but larger



Figure 5: **Question:** Which object in this image belongs to the category Herbivorous animals?

Answer Source: Image

Answer: Giraffe

Answer predicted: Giraffe



Figure 6: **Question:** What popular pet is in this image?

SPO triple: : {Goldfish, IsA, popular pet}

Answer Source: Image

Answer: Goldfish

Answer predicted: Fish



Figure 7: **Question:** What object in this image is commonly eaten for lunch?

SPO triple: : {Sandwich, IsA, meal commonly eaten for lunch}

Answer Source: Image

Answer: Sandwich

Answer predicted: Bread



Figure 8: **Question:** Where can you find the large object in the back of this image?

SPO triple: : {Bus, AtLocation, Bus stop}

Answer Source: Knowledge Base

Answer: Bus stop

Answer predicted: Wait place



Figure 9: **Question:** What can we find in the place shown in this image?

SPO triple: : {Furniture, AtLocation, Bedroom}

Answer Source: Knowledge Base

Answer: Furniture

Answer predicted: Your House

relevant answers being considered wrong.

Our model makes fewer mistakes when choosing among candidate entities for KVC since these entities tend to be atomic. Even so, entities sharing parent-child relationships could lead to multiplicity, as seen in Fig. 7 (the fact {Fish, IsA, popular pet} also exists in the KG). KB entities which can be free flowing text, tend to suffer from redundancy and semantic equivalence. This manifests as inaccuracies for the current baseline, as seen in Fig. 6 - 9. But this also points to the versatility of KG embeddings, that they have indeed learnt representations for each entity that is able to classify correct facts as true. We also see instances of our network performing multi-hop reasoning, as seen in Fig. 6. Our model predicts the answer as 'Bread', since the KG contains the facts {Bread, PartOf, Sandwich }, {Bread, Used-

For, Sandwich }. For a more thorough qualitative discussion, the interested reader is directed to the supplements section.

Conclusion

An architecture is proposed that solves the FVQA task even when the required edge is missing from the knowledge graph. In the process, we present the first approach to use KG embeddings for FVQA. Serendipitous benefits of the proposed approach include: (1) improved computational complexity (demonstrated in theory, but not measurable in practice), and (2) an improved representation of each image, as the span of KG embeddings of the visible entities. Future work might consider methods that combine global features via KG embeddings and local features via GCN for this task, in order to strengthen the KG-based entity embedding.



Figure 10: **Question:** Where is this place?

SPO triple: : {Life, AtLocation, Zoo}

Answer Source: Knowledge Base

Answer: Zoo

Answer predicted: in Zimbabwe

Ethical impact

We now examine the ethical implications of our work. A prominent issue could be that of different biases known to exist in our data sources. (Shankar et al. 2017) show population / representation bias existing in OpenImages and ImageNet. (Fisher et al. 2019) showed web-scale commonsense KGs can be tough to curate and can allow biases to creep in. (Janowicz et al. 2018) note how the density of world locations generating DBpedia data (extracted from Wikipedia) is at odds with world population density. Fig. 10 shows how this manifests in our system. The answer for a place relevant to giraffes in wildlife, comes up as Zimbabwe, even though the only edges present in the KG concerning Zimbabwe were {Person, AtLocation, in Zimbabwe}, {Dog, AtLocation, in Zimbabwe}, {Tree, AtLocation, in Zimbabwe}, {Elephant, AtLocation, in Zimbabwe}. Such an error is quite informative and humbling – this means that different modalities (image, language, graph) working in tandem could still amplify their individual biases. For deploying such a system, we recommend debiasing of parameters learned in our architecture. While ConceptNet has been active in debiasing their representations, debiasing KG embeddings has not received as much attention, and it could pose subtle problems given that most entities would have low node-degree. A multimodal approach to debias representations could be an interesting research direction.

References

Antol, S.; Agrawal, A.; Lu, J.; Mitchell, M.; Batra, D.; Zitnick, C. L.; and Parikh, D. 2015. VQA: Visual Question Answering. In *2015 IEEE International Conference on Computer Vision (ICCV)*, 2425–2433.

Auer, S.; Bizer, C.; Kobilarov, G.; Lehmann, J.; Ives, Z.; and et al. 2007. DBpedia: A Nucleus for a Web of Open Data. In *PROC. 6TH INT'L SEMANTIC WEB CONF.* Springer.

Bollacker, K.; Evans, C.; Paritosh, P.; Sturge, T.; and Taylor, J. 2008. Freebase: a collaboratively created graph database for structuring human knowledge. In *SIGMOD Conference*, 1247–1250.

Bordes, A.; Usunier, N.; Weston, J.; and Yakhnenko, O. 2013. Translating embeddings for modeling multi-relational data. In *In Advances in Neural Information Processing Systems 26. Curran Associates, Inc.*, 2787–2795.

Bordes, A.; Weston, J.; Collobert, R.; and Bengio, Y. 2011. Learning Structured Embeddings of Knowledge Bases. In *AAAI*.

Cai, L.; and Wang, W. Y. 2018. KBGAN: Adversarial Learning for Knowledge Graph Embeddings. In *Proceedings of the 2018 Conference of the North American Chapter of the Association for Computational Linguistics: Human Language Technologies, Volume 1 (Long Papers)*.

Dettmers, T.; Minervini, P.; Stenetorp, P.; and Riedel, S. 2018. Convolutional 2D knowledge graph embeddings. In Zilberstein, S.; McIlraith, S.; and Weinberger, K., eds., *Proc. AAAI*, 1811–1818.

Dong, X.; Gabrilovich, E.; Heitz, G.; Horn, W.; Lao, N.; Murphy, K. P.; Strohmann, T.; Sun, S.; and Zhang, W. 2014. Knowledge vault: a web-scale approach to probabilistic knowledge fusion. In *Knowledge Distillation and Data Mining*, 601–610. doi:10.1145/2623330.2623623.

Fisher, J.; Palfrey, D.; Christodoulopoulos, C.; and Mittal, A. 2019. Measuring Social Bias in Knowledge Graph Embeddings.

Galárraga, L.; Teflioudi, C.; Hose, K.; and Suchanek, F. M. 2013. AMIE: association rule mining under incomplete evidence in ontological knowledge bases. In *In WWW*.

Goyal, Y.; Khot, T.; Summers-Stay, D.; Batra, D.; and Parikh, D. 2017. Making the v in VQA Matter: Elevating the Role of Image Understanding in Visual Question Answering. In *Proceedings of the IEEE Conference on Computer Vision and Pattern Recognition (CVPR)*.

Gutmann, M.; and Hyvärinen, A. 2010. Noise-contrastive estimation: A new estimation principle for unnormalized statistical models. *Proceedings of Machine Learning Research*, 297–304. Chia Laguna Resort, Sardinia, Italy.

Guu, K.; Miller, J.; and Liang, P. 2015. Traversing Knowledge Graphs in Vector Space. In *Proceedings of the 2015 Conference on Empirical Methods in Natural Language Processing*, 318–327.

Halford, G. S.; Wilson, W. H.; and Phillips, S. 2010. Review Relational knowledge: the foundation of higher cognition.

He, K.; Zhang, X.; Ren, S.; and Sun, J. 2016. Deep Residual Learning for Image Recognition. *2016 IEEE Conference on Computer Vision and Pattern Recognition (CVPR)* 770–778.

Hochreiter, S.; and Schmidhuber, J. 1997. Long Short-Term Memory. *Neural Computation* 9(8): 1735–1780.

Janowicz, K.; Yan, B.; Regalia, B.; Zhu, R.; and Mai, G. 2018. Debiasing Knowledge Graphs: Why Female Presidents are not like Female Popes. In *Proceedings of the ISWC 2018 Posters & Demonstrations*.

Kipf, T. N.; and Welling, M. 2017. Semi-Supervised Classification with Graph Convolutional Networks. In *International Conference on Learning Representations (ICLR)*.

Lan, Z.; Chen, M.; Goodman, S.; Gimpel, K.; Sharma, P.; and Soricut, R. 2020. ALBERT: A Lite BERT for Self-supervised Learning of Language Representations. In *International Conference on Learning Representations*.

Li, X.; Taheri, A.; Tu, L.; and Gimpel, K. 2016. Commonsense Knowledge Base Completion. In *ACL (1)*.

Lin, T.-Y.; Dollar, P.; Girshick, R.; He, K.; Hariharan, B.; and Belongie, S. 2017. Feature Pyramid Networks for Object Detection. In *Proceedings of the IEEE Conference on Computer Vision and Pattern Recognition (CVPR)*.

Lin, T.-Y.; Maire, M.; Belongie, S.; Hays, J.; Perona, P.; Ramanan, D.; Dollár, P.; and Zitnick, C. 2014. Microsoft COCO: Common Objects in Context. *Lecture Notes in Computer Science* 8693: 740–755.

Liu, H.; and Singh, P. 2004. ConceptNet: A Practical Commonsense Reasoning Toolkit. *BT TECHNOLOGY JOURNAL* 22: 211–226.

Lu, J.; Yang, J.; Batra, D.; and Parikh, D. 2016. Hierarchical Question-Image Co-Attention for Visual Question Answering. In *Advances in Neural Information Processing Systems* 29, 289–297.

Malaviya, C.; Bhagavatula, C.; Bosselut, A.; and Choi, Y. 2020. Commonsense Knowledge Base Completion with Structural and Semantic Context. *Proceedings of the 34th AAAI Conference on Artificial Intelligence*.

Mitchell, T.; and Fredkin, E. 2014. Never-ending language learning. In *2014 IEEE International Conference on Big Data (Big Data)*, 1–1.

Narasimhan, M.; Lazebnik, S.; and Schwing, A. 2018. Out of the Box: Reasoning with Graph Convolution Nets for Factual Visual Question Answering. In *Advances in Neural Information Processing Systems* 31, 2654–2665.

Narasimhan, M.; and Schwing, A. G. 2018. Straight to the Facts: Learning Knowledge Base Retrieval for Factual Visual Question Answering. *CoRR*.

Nickel, M.; Tresp, V.; and Kriegel, H. 2011. A Three-Way Model for Collective Learning on Multi-Relational Data. In *Proc. International Conference on Machine Learning*.

Pennington, J.; Socher, R.; and Manning, C. 2014. GloVe: Global Vectors for Word Representation. In *Proceedings of the 2014 Conference on Empirical Methods in Natural Language Processing (EMNLP)*, 1532–1543.

Ren, S.; He, K.; Girshick, R.; and Sun, J. 2015. Faster R-CNN: Towards Real-Time Object Detection with Region Proposal Networks. In *Advances in Neural Information Processing Systems* 28, 91–99.

Russakovsky, O.; Deng, J.; Su, H.; Krause, J.; Satheesh, S.; Ma, S.; Huang, Z.; Karpathy, A.; Khosla, A.; Bernstein, M.; Berg, A. C.; and Fei-Fei, L. 2015. ImageNet Large Scale Visual Recognition Challenge. *International Journal of Computer Vision (IJCV)*.

Shankar, S.; Halpern, Y.; Breck, E.; Atwood, J.; Wilson, J.; and Sculley, D. 2017. No Classification without Representation: Assessing Geodiversity Issues in Open Data Sets for the Developing World. In *NIPS 2017 workshop: Machine Learning for the Developing World*.

Simonyan, K.; and Zisserman, A. 2015. Very Deep Convolutional Networks for Large-Scale Image Classification. In *Proc. International Conference on Learning Representations*.

Socher, R.; Chen, D.; Manning, C.; and Ng, A. 2013. Reasoning with Neural Tensor Networks for KnowledgeBase Completion. In *Advances in Neural Information Processing Systems*, 926–934. Curran Associates, Inc.

Suchanek, F. M.; Kasneci, G.; and Weikum, G. 2007. Yago: A Core of Semantic Knowledge. In *IN PROC. OF WWW '07*, 697–706. ACM.

Sun, Z.; Deng, Z.-H.; Nie, J.-Y.; and Tang, J. 2019. RotatE: Knowledge Graph Embedding by Relational Rotation in Complex Space. In *Proc. International Conference on Learning Representations*, 1–18.

Tandon, N.; de Melo, G.; Suchanek, F. M.; and Weikum, G. 2014. WebChild: harvesting and organizing commonsense knowledge from the web. In *Seventh ACM International Conference on Web Search and Data Mining, WSDM 2014, New York, NY, USA, February 24-28, 2014*, 523–532.

Trouillon, T.; Welbl, J.; Riedel, S.; Gaussier, E.; and Bouchard, G. 2016. Complex Embeddings for Simple Link Prediction. *Proceedings of Machine Learning Research*, 2071–2080. New York, New York, USA: PMLR.

Wang, P.; Wu, Q.; Shen, C.; Dick, A.; and van den Hengel, A. 2018. FVQA: Fact-Based Visual Question Answering. volume 40, 2413–2427.

Wu, Q.; Shen, C.; Liu, L.; Dick, A.; and Van Den Hengel, A. 2016. What Value Do Explicit High Level Concepts Have in Vision to Language Problems? In *2016 IEEE Conference on Computer Vision and Pattern Recognition (CVPR)*, 203–212.

Zagoruyko, S.; and Komodakis, N. 2016. Wide Residual Networks. In *BMVC*.

ZFTurbo. 2018. Keras-RetinaNet for Open Images Challenge 2018. <https://github.com/ZFTurbo/Keras-RetinaNet-for-Open-Images-Challenge-2018.git>.

Zhou, B.; Lapedriza, A.; Khosla, A.; Oliva, A.; and Torralba, A. 2017. Places: A 10 million Image Database for Scene Recognition. *IEEE Transactions on Pattern Analysis and Machine Intelligence*.